

High-spin structure and Band Termination in ^{103}Cd

A. Chakraborty¹, Krishichayan, S. Mukhopadhyay, S. Ray, S.N. Chintalapudi, S.S. Ghugre, N.S. Pattabiraman², and A.K. Sinha
*UGC - DAE Consortium for Scientific Research, Kolkata Center,
 Sector III/LB-8, Bidhan Nagar, Kolkata 700098, India*

S. Sarkar³

Department of Physics, Bengal Engineering and Science University, Shibpur, Howrah 711103, India

U. Garg and S. Zhu⁴

Department of Physics, University of Notre Dame, Notre Dame, IN 46556, USA

M. Saha Sarkar

*Saha Institute of Nuclear Physics, Sector-I/AF, Bidhan Nagar, Kolkata 700064, India**

Excited states of the neutron deficient ^{103}Cd nucleus have been investigated via the $^{72}\text{Ge}(^{35}\text{Cl}, \text{p}3\text{n})$ reaction at beam energy of 135 MeV by use of in-beam spectroscopic methods. Gamma rays depopulating the excited states were detected using the Gammasphere spectrometer with high-fold γ -ray coincidences. A quadrupole γ -ray coincidence analysis (γ^4) has been used to extend the known level scheme. The positive parity levels have been established up to $J = 35/2\hbar$ and $E_x = 7.071$ MeV. In addition to the observation of highly-fragmented level scheme belonging to the positive-parity sequences at $E_x \sim 5$ MeV, the termination of a negative-parity sequence connected by $E2$ transitions has been established at $J = 47/2\hbar$ and $E_x = 11.877$ MeV. The experimental results corresponding to both the positive- and negative-parity sequences have been theoretically interpreted in the framework of the core particle coupling model. Evidence is presented for a shape change from collective prolate to non-collective oblate above the $J^\pi = 39/2^-$ (8011 keV) level and for a smooth termination of the negative-parity band.

PACS numbers: 27.60.+j, 23.20.Lv, 21.60.Ev

I. INTRODUCTION

The level structures of cadmium isotopes exhibit a variety of appealing features with the variation in the neutron number. The chain of isotopes with $A \leq 102$ indicate single particle behavior resulting from the excitations of proton holes and the neutron particles across the doubly magic $Z = N = 50$ core. The level structures of $^{98,99}\text{Cd}$, lying in the vicinity of ^{100}Sn , have been the focus of several experimental investigations [1, 2, 3, 4]. These studies are expected to furnish information on the single-particle energies and two-body matrix elements which would help develop better empirical interactions for the model valence spaces around the $N = Z = 50$ magic shell closure. While the “fingerprint” of core excitations or excitations involving $1h_{11/2}$ neutrons have been demonstrated in ^{100}Cd from the observation of high-energy transitions ($E_\gamma \sim 2.0 - 2.6$ MeV) around the $I = 14\hbar$ [5]; a theoretical prediction for the ground state of the nucleus ^{104}Cd to be a superposition of prolate ($\beta_2 \sim 0.15$) and oblate ($\beta_2 \sim -0.12$) configurations has also been mentioned in Ref. [6]. With the increase in neutron number ($A = 106 - 110$), shears mechanism appears to develop in Cd-isotopes due to the availability of proton holes in the high- Ω $1g_{9/2}$ orbitals and neutron particles in the low- Ω $1g_{7/2}/2d_{5/2}$ and $1h_{11/2}$ orbitals, leading to magnetic and anti-magnetic rotations [7, 8, 9, 10, 11]. Further, for a long time, cadmium isotopes lying close to stability line ($111 \leq A \leq 114$) have been considered as examples of quadrupole

^{*1}Present address: *Department of Physics, Krishnath College, Berhampore 742101, India*; ²Present address: *Department of Physics, University of York, York YO10 5DD, UK*; ³On lien from *Department of Physics, The University of Burdwan, Burdwan 713104, India*; ⁴Present address: *Physics Division, Argonne National Laboratory, Argonne, Illinois 60439*

vibrator with spherical shape [12]. Also during the past decade, Cd isotopes have emerged as the laboratory for the study of multi-phonon excitations, such as the three-quadrupole-phonon [13, 14, 15] and mixed quadrupole-octupole excitations of the type $(2^+ \otimes 3^-)$ [16, 17, 18]. The observation of one-phonon mixed-symmetry state [19] also adds to the diversity of excitation modes in Cd isotopes.

The ^{103}Cd nucleus, with two proton holes and five valence neutrons, with respect to the ^{100}Sn core, lies in the upper part of the $1g_{9/2}$ proton sub-shell and in the lower part of the gds neutron sub-shell. This is a transitional region between the spherical nuclei close to the doubly magic nucleus ^{100}Sn and the deformed nuclei with more valence particles. The prolate deformation-driving character of the low- Ω $h_{11/2}$ orbitals, however, allows the formation of quasi-rotational bands in such nuclei. The relatively small number of available valence particles implies that these quasi-rotational bands would terminate at rather low spins that can be accessed experimentally.

Excited states in ^{103}Cd have been previously investigated by several groups [20, 21, 22]. The first excited state in ^{103}Cd with $J^\pi = 7/2^+$ at $E_x = 188$ keV was established by Lhersonneau *et al.* [20] following the β -decay of ^{103}In . Two high-spin studies have also been reported in the subsequent years [21, 22]. The present work is aimed at extending the available information on the excited states of ^{103}Cd up to the energy and spin regime where one would expect termination of bands, and also to explore the interplay between the single particle and deformed structures. Apart from a significant extension of the positive-parity level sequences up to $J^\pi = (35/2^+)$ and $E_x \sim 7$ MeV, the present investigation has furnished evidence for a smooth termination of the negative-parity decoupled band. The phenomenological core particle coupling model (CPCM) has been employed to understand the microscopic properties of the level structures and other spectroscopic observables.

II. EXPERIMENTAL PROCEDURE AND DATA ANALYSIS

The experiment was performed with the $^{72}\text{Ge}(^{35}\text{Cl}, p3n)^{103}\text{Cd}$ reaction, using a 135-MeV ^{35}Cl beam provided by the ATLAS facility at the Argonne National Laboratory. The ^{72}Ge target (of 1 mg/cm² thickness) was evaporated onto a 15 mg/cm²-thick gold foil; the choice of backing provided sufficient stopping power to slow down and stop the recoiling nuclei produced in this reaction. A thin (40 $\mu\text{g}/\text{cm}^2$) Al layer was evaporated between the target and the backing to avoid migration of target material into the backing.

The de-exciting γ -rays were detected using the Gammasphere spectrometer [23, 24, 25] in the stand alone mode. Events were written on magnetic tape when at least three suppressed Ge detectors in the array detected γ rays within the prompt coincidence time window. A total of approximately 2×10^9 “triple coincidence” events were recorded during the experiment. The coincidence events were sorted into a γ^4 histogram and asymmetric angle - selected matrices (see below) for off-line analysis. The data analysis was performed using the Linux based software packages IUCSORT [26, 27] and RADWARE [28].

The other strongly populated nuclei with $A \sim 100$ in the present experiment are $^{100,101}\text{Pd}$, $^{103,104}\text{Ag}$ and ^{104}Cd . The high-fold coincidence data helped us to unambiguously place in the level scheme of ^{103}Cd some transitions that are identical in energy to those from the aforementioned neighboring evaporation residues.

Multipolarities of emitting γ -rays from ^{103}Cd were deduced from the analysis of Directional Correlations of γ -rays de-exciting Oriented states (DCO ratio method) [29]. The method is based on the observed coincidence intensity anisotropy, obtained from the angle dependent $\gamma - \gamma$ coincidence. This anisotropy ratio is denoted by R_{DCO} . In order to extract DCO-ratios, the coincidence data were sorted into an asymmetric matrix whose one axis corresponded to the γ -ray energy deposited in the detectors at 35° and 145° and the other axis corresponded to the γ -ray energy deposited in the detectors at 90° . The DCO-ratios are, then, defined as:

$$R_{DCO} = \frac{I_{\gamma_1 \text{ at } 35^\circ \text{ and } 145^\circ; \text{ gated with } \gamma_2 \text{ at } 90^\circ}}{I_{\gamma_1 \text{ at } 90^\circ; \text{ gated with } \gamma_2 \text{ at } 35^\circ \text{ and } 145^\circ}}$$

The DCO ratios were at first calibrated by measuring several known $E2$ and dipole transitions in ^{100}Pd [30] and ^{101}Pd [31], which were also populated in the present experiment. Gating on a stretched quadrupole transition γ_2 , one obtains value of $R_{DCO} \sim 1.0$ for a stretched quadrupole transition, and ~ 0.5 for a stretched pure dipole. By gating on a stretched pure dipole transition, one would get ~ 2.0 for a quadrupole and ~ 1.0 for a pure dipole transition. For mixed dipole/quadrupole γ_2 transitions, R_{DCO} depends on the value of the mixing ratio.

In assigning spins and parities to the observed levels, we have assumed that the stretched quadrupole transitions are of $E2$ multipolarity (in general), the pure dipoles can have either $E1$ or $M1$ character, and the mixed transitions are of $M1/E2$ type. Although the DCO-ratios can not distinguish between stretched $E2$'s and $\Delta I = 0$ dipoles or certain $\Delta I = 1$ admixtures, the spin assignments are relatively unambiguous since the ^{103}Cd level scheme is quite complex with many parallel decay pathways and many cross-over connections. Here, we have used the general yrast argument that levels populated in heavy-ion reactions usually have spins increasing with increasing excitation energy.

Although for most of the transitions, the DCO-ratios have been obtained using the gating transition with known multipolarity, the same procedure could not be utilized to determine the DCO-ratios for the weak transitions lying above ~ 5 MeV excitation. The multiplicities of such transitions have been inferred from the measured DCO-ratios of the known intense transitions, lying below ~ 5 MeV excitation, with the corresponding weak transition used as the gating transition in the DCO analysis.

III. EXPERIMENTAL RESULTS

The ^{103}Cd level scheme resulting from the analysis of the coincidence γ^4 histogram is shown in Figs. 1 and 2. In the figures, the energies of the γ transitions are labeled in keV and the widths of the arrows are approximately proportional to the transition intensities. The main positive-parity sequence has been extended up to an excitation energy of ~ 7 MeV (with $J^\pi = (35/2^+)$) and the negative-parity sequence is extended up to ~ 12 MeV (with $J^\pi = (47/2^-)$). About 50 new transitions have been placed in the level scheme. Several level sequences have been labeled (I,II,III,IV) to facilitate further discussion.

Typical prompt $\gamma\gamma\gamma\gamma$ coincidence spectra for positive-parity levels in ^{103}Cd are shown in Fig. 3. Fig. 4(a-b) depicts the representative γ^4 coincidence spectrum for the transitions belonging to negative parity sequence (*Seq IV*). The newly observed weak transitions feeding the $39/2^-$ level at 8011 keV are clearly seen in the figure. The presence of the top most 2171-keV transition of *Seq IV* could be identified from a sum of single-gated γ -ray coincidence spectra with the gates set on 901-, 1063-, and 1234-keV transitions (see Fig. 4(c)). A similar procedure has been adopted in Refs. [32, 33] to assign weak transitions belonging to the corresponding level schemes. However, Fig. 4(b) does not indicate the presence of any transition with energy more than 1.6 MeV; the 2171-keV transition has, therefore, been placed in the level scheme only as tentative.

The main positive-parity sequence (*Seq I*) is built on the $5/2^+$ ground state. Both positive-parity sequences (*Seq I* and *III*) exhibit an irregular and complex structure above 4 MeV, a feature typical of particle-hole excitations in nearly-spherical nuclei. The negative-parity sequence (*Seq IV*) built on the $11/2^-$ bandhead at $E_x = 1.671$ MeV exhibits a regularity up to $J^\pi = 39/2^-$ and $E_x = 8.011$ MeV. Above this state, a certain regularity persists, though weakly, up to $J^\pi \sim (47/2^-)$ at $E_x = 11.877$ MeV. However, the level structure appears to gradually become irregular around $E_x \sim 6.8$ MeV, likely indicating a change in structure.

Numerous cross-over transitions, established from the observed coincidence relations, provide checks for the placement and ordering of transitions in many cases in the complex scheme. The placement of all the known transitions is in agreement with the previous work [22]. In addition to the extension of the existing level scheme, the present investigation also leads to the unambiguous placement of some of the transitions, which were tentatively placed in the work of Palacz *et al.* [22]. As there are a number of doublets present in the level scheme, different gates have been used to determine their relative intensities and DCO-ratios.

The 1128-keV transition, which appears to belong to *Seq I* could not be convincingly placed in the level scheme. Also the 262- and 373-keV transitions, which appear to be in coincidence with the 1573-keV and other transitions in the cascade, could not be placed in the level scheme due to the poor statistics. Furthermore, the 1040-keV transition could not be placed in the level scheme although it appears to be in strong coincidence with 259-keV and the other low-lying transitions of *Seq I*. There seems to be a linking between the 1234-keV (*Seq IV*) and 1609-keV (*Seq I*) transitions; however, the coincidence relationship between the two could not be established from the present data.

The γ -ray energies, intensities, DCO-values, and multiplicities for the transitions assigned to ^{103}Cd have been summarized in Table I. The uncertainties in the γ -ray energies correspond to the error due to peak fitting. The uncertainties in the intensities encompass errors due to background subtraction, peak fitting, statistical fluctuations, and efficiency correction; the error bars may have been somewhat underestimated for the weakest transitions. The uncertainties quoted in the DCO-ratios include the errors due to background subtraction, statistical fluctuations, and peak fitting.

Although the intensity balance between the transitions feeding to and decay out from a particular level is equal within error for most of the cases, there is a marked deviation observed for the level with $J^\pi = 19/2^+$. This level was found to be isomeric in the work of Palacz *et al.* [22]. A large intensity imbalance between feeding and decay has similarly been observed for the $27/2^+$ level at 4025 keV.

IV. THEORETICAL CALCULATIONS AND DISCUSSION

The experimental level structure of ^{103}Cd (see Figs. 1 and 2) consists of three positive-parity sequences (*Seq I - III*) and a negative-parity band (*Seq IV*) built on $J^\pi = 11/2^-$ state.

Meyer *et al.* [21] suggested that the low-lying yrast positive-parity levels are the members of a decoupled band, built on the first excited $7/2^+$ level, with the odd $\nu(1g_{7/2})$ quasi-particle coupled to the core. This was based on the similarity of the excitation energies of the $11/2^+$, $15/2^+$, $19/2^+$, levels in ^{103}Cd to the 2^+ , 4^+ , 6^+ , levels of the respective ground state bands in $^{102,104}\text{Cd}$. For a complete decoupled band [34] built on $7/2^+$ band head, the excitation energies of the levels belonging to the sequence (with signature, $\alpha = -1/2$) $11/2^+$, $15/2^+$, $19/2^+$, should be lower than their respective unfavored signature ($\alpha = +1/2$) partners $9/2^+$, $13/2^+$, $17/2^+$, The levels corresponding to the unfavored signature partners are populated weakly in heavy-ion reactions and in many cases can not be observed experimentally. As Meyer *et al.* [21] had not observed the unfavored signature partners, it supported their conclusion for considering the positive parity band with $7/2^+$ band head as the decoupled band.

In the subsequent work of Palacz *et al.* [22], as well as in the present investigation, the unfavored signature partners have been observed. It is found that although the signature splitting is strong, the unfavored signature partners are still energetically lower than the corresponding next favored ones and hence the band is not completely decoupled.

The experimental level energies of the negative-parity band are also found to be in close agreement with those of the corresponding levels of the ground state bands of $^{102,104}\text{Cd}$. This suggests that the excited negative-parity levels in ^{103}Cd originate essentially due to the coupling of the $1h_{11/2}$ neutron quasiparticle with the collective excitations of the ^{102}Cd or ^{104}Cd core. As such, the observed negative-parity band is identified as a decoupled band arising from $\nu h_{11/2}$ Nilsson orbits with the Fermi level lying near a low- Ω orbital ($\Omega = 1/2$ in the present case).

From the shell model point of view, ^{103}Cd nucleus can be thought of as having two proton-holes $\pi(1g_{9/2})^{-2}$ and five neutrons in the $\nu(2d_{5/2}, 1g_{7/2}, 3s_{1/2}, 2d_{3/2}, 1h_{11/2})$ valence space with respect to doubly magic $^{100}\text{Sn}_{50}$ core. The $5/2^+$ ground state and the low-lying positive parity excited states up to $21/2^+$ can be built from the $[\pi(g_{9/2})^{-2} \otimes \nu(d_{5/2})^{-1}]$ multiplet. Beyond $21/2^+$, neutron excitations to $1g_{7/2}$ orbital are essential. This can provide a maximum J^π of $39/2^+$. The maximum J^π that can be built in the $[\pi(g_{9/2}), \nu(gdsh)]$ valence space is $55/2^+$ which comes from the $[\pi(g_{9/2})^{-2} \otimes \nu(g_{7/2}h_{11/2}^4)]$ configuration. Observed maximum spin is then, $35/2$ for the positive parity. There are a large number of configurations belonging to the partitions $[\pi(g_{9/2})^{-2}\nu(gdsh)^5]$. Most of the states can be built in a variety of ways. Therefore, the underlying structure of most of the levels is expected to consist of admixture of configurations of many multi-particle-hole excitations. This gives rise to a complex and irregular structure beyond the first $21/2^+$ state belonging to the energetically lowest configuration $[\pi(g_{9/2})^{-2} \otimes \nu(d_{5/2})^{-1}]$. For the positive parity levels with $J^\pi > 21/2^+$, $\nu(d_{5/2})^{-1} \rightarrow \nu(gdsh)$ excitations are needed and they appear at ≥ 4 MeV. This can be estimated from the consideration of the single particle energies [22] of the valence orbitals and the expected configuration mixing consisting of energetically higher lying configurations. This qualitative picture for the positive parity levels has actually been observed in the shell model calculations by Palacz *et al.* [22]. They showed that the positive-parity levels were highly configuration mixed. Further, β_2 values of even Cd-isotopes with $A \geq 102$ are known to lie in the range 0.17 - 0.19 [35]. Thus, one might expect a small deformation in ^{103}Cd and, consequently, the onset of mild collectivity. The regularity observed in the negative-parity band could not be reproduced in shell model calculations even with large valence basis space considered by Palacz *et al.* [22].

The possibility of a mild deformation in ^{103}Cd makes the Core Particle Coupling Model (CPCM), proposed by Muller and Mosel [36, 37], an ideal choice to interpret the observed excitation modes. The CPCM employed here has the added advantage that the experimental level energies of the core can be directly used as inputs. As the core simulation is not needed, the approach is especially suitable for very weakly deformed systems where variable moment of inertia (VMI) or constant moment of inertia (CMI) approaches within the standard particle rotor model fail due to the non-rotational nature of the core.

The CPCM calculations were performed for the positive as well as negative-parity energy levels using both ^{102}Cd and ^{104}Cd cores. Similar energy eigenvalues were obtained for most of the levels in ^{103}Cd with both the cores. This was possible with a slight adjustment of the attenuation factor of the Coriolis matrix element, keeping all other parameters the same. But the level energies as well as the transition probabilities of the higher-spin levels appear to be better reproduced with the ^{102}Cd core and, hence, only the results of the calculations performed with the ^{102}Cd core are being presented.

All the parameters used for the CPCM calculation for the positive parity levels are listed in Table II. The Nilsson single particle orbitals for the neutron *viz.* $3s_{1/2}$, $2d_{3/2}$, $2d_{5/2}$, $1g_{7/2}$, and $1g_{9/2}$, belonging to $N = 4$ oscillator shell were considered for the calculation of positive-parity levels. The neutron Fermi level lies near the $3/2^+[411]$ and $5/2^+[413]$ Nilsson orbitals, originating predominantly from $1g_{7/2}$ and $2d_{5/2}$, respectively. The pairing gap parameter Δ was estimated from the experimental odd-even mass difference and is similar to the value obtained from the expression $\Delta = 12/A^{1/2}$. It is generally observed that the use of Δ value obtained from the experimental odd-even mass difference results in an overestimation of the Coriolis interaction, requiring comparatively larger Coriolis attenuation coefficients (see Table II). The experimental core (^{102}Cd) energies from 0^+ to 14^+ states [38] were supplied as inputs. Since the experimental energies in ^{102}Cd are available only up to $J^\pi=14^+$, the energies of the higher lying levels (16^+ - 30^+) of the core were obtained from a fit $[E(R) = a + bR + cR^2]$ to the low-lying known levels and were also fed in as

inputs; here, R denotes the spin of a particular level of the core and $E(R)$ is the energy of the corresponding level. The large b/c ratio ($=31.6$), obtained from the fitting, and the value of $R_4(= E_{4+} / E_{2+} = 2.1)$ are indicative of a vibrational nature of the core.

The $M1$ transition rates have been calculated using $(g_{\nu}^s)_{free} = -3.826$, $(g_{\nu}^l) = 0.0$, and $g_R(= Z/A_{core}) = 0.47$. For the calculation of $B(E2)$ values, the multiplicative factor for the effective charge for the quasineutron is 0.5 [39]. The contribution of the core is included through the intrinsic quadrupole moment Q_0 using the relation given in Ref. [35].

The negative-parity levels have been calculated using the same Nilsson parameters as those used for the positive-parity levels with the attenuation of the Coriolis matrix elements by a factor of 0.97. Only the neutron Nilsson orbitals originating from the spherical single particle $1h_{11/2}$ orbital, belonging to $N = 5$ major shell, were included in our calculations. Calculations were also carried out for the case of oblate deformation ($\delta = -0.14$), keeping all other parameters unchanged. The results of all these calculations are discussed below.

A. Positive-parity Sequences

Theoretical energy eigenvalues for the positive-parity states obtained from CPCPM calculation are compared with the experimental results in Fig. 5. The calculations successfully reproduce the observed ordering, energy spacing and the signature splitting of the levels.

The $5/2^+$ ground state is found to be dominated by the Nilsson basis states $3/2[422]$ ($= 76\% \nu d_{5/2}$) and $5/2[413]$ ($= 86\% \nu d_{5/2}$) contributing about 18% and 67%, respectively. Basis states involving $\nu g_{7/2}$ also have non-negligible contributions; the contributions from the $3/2[411]$ ($= 81\% \nu g_{7/2}$) and $1/2[420]$ ($= 55\% \nu g_{7/2}$) Nilsson states are about 4.4% and 4%, respectively. The structure of the other members of the yrast $(+, +1/2)$ group of $\Delta I=2$ levels (except the $9/2^+$ state) are mostly dominated by $1/2[420]$ and $3/2[411]$ basis states and the $13/2^+$ state is an almost pure $3/2[411]$ state. The yrast $9/2^+$ state, the first excited state of this group, appears to be highly mixed with sizeable contributions from the close-lying $5/2[413]$ (20%), $3/2[422]$ (30%), $1/2[420]$ (12%) and $3/2[411]$ (20%) $\nu g_{7/2}$ orbitals.

The yrast $7/2^+$ level originates predominantly from the $1/2[420]$ (29%) and $3/2[411]$ (46%) orbitals, with admixtures from $5/2[402]$ ($= 89\% \nu g_{7/2}$) (8.41%), $1/2[411]$ ($= 30\% \nu g_{7/2}$) (7.29%) and $1/2[411]$ ($= 38\% \nu s_{1/2}$) (7.29%). Other members of the yrast $(+, -1/2)$ group of levels up to $35/2^+$ (except the $11/2^+$ level) have a major contribution from $3/2[411]$ orbital; the $11/2^+$ level originates predominantly from $3/2[411]$ (58%) and $1/2[420]$ (26%).

It is interesting to understand the significance of the agreement of the CPCPM results with the experiment. The positive parity levels which are supposed to originate from the admixture of a large number of configurations belonging to $[\pi(g_{9/2})^{-2} \nu(gdsh)^5]$ partitions can in effect be decomposed into collective excitations (of ^{102}Cd) based on the configuration mixing of states belonging to $[\pi(g_{9/2})^{-2} \otimes \nu(gdsh)^4]$ configurations of the ^{102}Cd core, coupled to a neutron in gds orbitals.

The model wavefunctions were used to calculate electromagnetic transition rates. The experimental and theoretical branchings for the levels have been compared in Table III. It may be noted that the trend of the observed branchings for most of the levels could be reproduced in the present calculations. This validates the wavefunctions obtained in the calculations and further corroborates the underlying structure assumption of the levels, *i.e.*, a neutron quasiparticle coupled to the collective excitation modes of the ^{102}Cd core. The discrepancy between the predicted and experimental values of the branching ratios for levels with $E_x \geq 4$ MeV might be attributable to the unobserved transitions feeding the $27/2^+$ level at 4025 keV; a large intensity imbalance between the feeding and decay pattern for this level supports this conjecture.

B. Negative-parity Sequence

The decay of the negative parity states, belonging to *Seq IV*, is dominated by sequences of $E2$ transitions between rather regularly spaced levels. The onset of this regular pattern can be traced to the neutron excitation to the $\nu h_{11/2}$ orbital, which is mandatory to generate the observed negative parity levels. The shape driving properties of the intruder $\nu h_{11/2}$ orbital are obvious with the appearance of regularity in the level scheme at relatively low excitation.

The negative-parity levels up to $J^\pi = 39/2^-$ are connected by strong interband transitions. However, above the $J^\pi = 35/2^-$ level at $E_x = 6777$ keV, the level scheme exhibits an irregular pattern with several parallel feeding transitions. These transitions are extremely weak. The remarkable dissimilarity in levels above and below the $J^\pi = 35/2^-$ state is suggestive of a change in the level structure at high spins. The fragmentation of intensity into parallel cascades above the $35/2^-$ state could be attributed to the contribution of other particle-hole excitations. This conjecture, based on the phenomenological observations, is also corroborated by the CPCPM and TRS calculations (discussed below in this section).

The negative-parity band persists, although weakly, up to the $(47/2^-)$ level at 11877 keV. If the negative-parity band is based on the $\pi(g_{9/2})^{-2} \otimes \nu(g_{7/2}d_{5/2})^4(h_{11/2})^1$ configuration, this is expected to generate a maximum angular momentum of $47/2^-$, which, indeed, corresponds to the highest observed spin in this band. This may be understood as the termination of the band at $J^\pi = (47/2^-)$.

A comparison of the predictions of the CPCM with the observed excitation energies is presented in Fig. 6. These calculations were carried out assuming both prolate and oblate deformation for the ^{102}Cd core. The Nilsson basis states for the underlying levels obtained in these calculations have been described in the caption of Fig. 6.

The theory predicts reasonably well the experimental spectra up to the $39/2^-$ level for prolate deformation. However, the same could not be reproduced with the consideration of an oblate deformation of the core. For higher spins ($> 39/2^-$), the calculation with oblate deformation seems to be in better agreement. Thus, there likely is a shape change from prolate to oblate above the $J^\pi = 39/2^-$ level at $E_x = 8011$ keV in the vicinity of the band termination, which is corroborated by the Total Routhian Surface (TRS) calculations. These calculations also indicate (see Fig. 7) the evolution of shape from collective prolate ($\gamma \sim 10^\circ$) to non-collective oblate ($\gamma \sim 60^\circ$) as the rotational frequency increases. Hence the CPCM and TRS calculations both point towards the transition from prolate shape to oblate shape as the excitation energy increases.

To further investigate the terminating nature of the $\Delta I=2$ negative-parity band, we have plotted in Fig. 8 the dynamic moment of inertia $J^{(2)}$ [40] as a function of rotational frequency for this band. In the figure, variation of $J^{(2)}$ with rotational frequency for the *Seq IV* in ^{103}Cd is compared with that for a rigid rotor with $\beta_2 = 0.23$ [40]. The negative value of $J^{(2)}$ at $\hbar\omega = 0.42$ MeV indicates backbending, as also discussed in Ref. [22]. Beyond this $\hbar\omega$ value, $J^{(2)}$ decreases smoothly with increase in $\hbar\omega$. At the top of the band, $J^{(2)}$ is about one fourth of the rigid rotor value. This is a general feature for the decoupled smooth terminating bands observed in $A = 110$ region [32, 33, 41, 42]. However, a comparison of the observed variation of $J^{(2)}$ in ^{103}Cd with the case of other terminating bands in the $A = 100$ [40, 43] and $A = 155 - 160$ [40, 44] regions show a distinct difference. In contrast to the observed irregular behavior of $J^{(2)}$ with rotational frequencies for those nuclei, the $J^{(2)}$ in ^{103}Cd appears to be rather smooth. This smooth variation and the decreasing trend of $J^{(2)}$ in ^{103}Cd is further indicative of a gradual loss of collectivity and possible change over to oblate shape. It might be surmised, that the observed band termination for the negative-parity sequence corresponds to a “smooth termination”.

V. CONCLUSIONS

The neutron-deficient nucleus ^{103}Cd has been studied to the high-spin regime by means of in-beam γ -ray spectroscopy using Gammasphere. More than fifty new transitions have been found and placed in the level scheme. This has led to a substantial extension of both the positive- and negative-parity sequences. The decoupled negative parity sequence connected through the cascade of $E2$ transitions has been observed up to the terminating $47/2^-$ state. The core particle coupling model reproduces both the positive- and negative-parity sequences reasonably well. Both phenomenology, CPCM and TRS calculations provide evidence for a likely transition from prolate to oblate structure at $J^\pi > 39/2^-$ and for the termination of the negative-parity band; this termination resembles the “smooth terminating bands” previously observed in the $A = 110$ region. Further experimental and theoretical work is required to confirm the smooth terminating nature of the negative parity sequence (*Seq IV*). Experimental lifetime information of the levels in *Seq IV* for reliable determination of transition quadrupole moments (Q_t values) would be particularly important to conclude firmly about the nature of this sequence.

VI. ACKNOWLEDGMENTS

We wish to thank Drs. M.P. Carpenter, R.V.F. Janssens, B. Kharraja, F.G. Kondev, and T. Lauritsen for their help with the Gammasphere experiment and for many fruitful discussions. The help received from Dr. G. Mukherjee with the TRS calculation is also gratefully acknowledged. This work was supported in part by the National Science Foundation (Grants No. INT-01115336 and PHY04-57120) and the University Grants Commission, Government of India.

-
- [1] M. Górska *et al.*, Phys. Rev. Lett. **79**, 2415 (1997).
 - [2] M. Lipoglavšek *et al.*, Nucl. Phys. **A682**, 399c (2001).
 - [3] M. Lipoglavšek *et al.*, Phys. Rev. C **66**, 011302(R) (2002).
 - [4] A. Blazhev *et al.*, Phys. Rev. C **69**, 064304 (2004).
 - [5] R.M. Clark *et al.*, Phys. Rev. C **61**, 044311 (2000).
 - [6] G.A. Müller *et al.*, Phys. Rev. C **64**, 014305 (2001).
 - [7] A.J. Simons *et al.*, Phys. Rev. Lett. **91**, 162501 (2003).
 - [8] C.J. Chiara *et al.*, Phys. Rev. C **61**, 034318 (2000).
 - [9] N.S. Kelsall *et al.*, Phys. Rev. C **61**, 011301(R) (1999).
 - [10] P. Datta *et al.*, Phys. Rev. C **71**, 041305(R) (2005).
 - [11] R.M. Clark *et al.*, Phys. Rev. Lett. **82**, 3220 (1999).
 - [12] J.R. Comfort, C.K. Bockelman, and P.D. Barnes, Phys. Rev. **157**, 1065 (1967).
 - [13] A. Aprahamian, D.S. Brenner, R.F. Casten, R.L. Gill, and A. Piotrowski, Phys. Rev. Lett. **59**, 535 (1987).
 - [14] R.F. Casten, J. Jolie, H.G. Börner, D.S. Brenner, N.V. Zamfir, W.-T. Chou, and A. Aprahamian, Phys. Lett. **B297**, 19 (1992).
 - [15] H. Lehmann, P.E. Garrett, J. Jolie, C.A. McGrath, Minfang Yeh, and S.W. Yates, Phys. Lett. **B387**, 259 (1996).
 - [16] A. Gade, J. Jolie, and P. von Brentano, Phys. Rev. C **65**, 041305(R) (2002).
 - [17] D. Bandyopadhyay, C.C. Reynolds, S.R. Leshner, C. Fransen, N. Boukharouba, M.T. McEllistrem, and S.W. Yates, Phys. Rev. C **68**, 014324 (2003).
 - [18] P.E. Garrett, H. Lehmann, J. Jolie, C.A. McGrath, Minfang Yeh, and S.W. Yates, Phys. Rev. C **59**, 2455 (1999).
 - [19] D. Bandyopadhyay, C.C. Reynolds, C. Fransen, N. Boukharouba, M.T. McEllistrem, and S.W. Yates, Phys. Rev. C **67**, 034319 (2003).
 - [20] G. Lhersonneau, G. Dumont, K. Cornelis, M. Huyse, and J. Verplancke, Phys. Rev. C **18**, 2688 (1978).
 - [21] M. Meyer, R. Beraud, A. Charvet, R. Duffait, J. Treherne, and J. Genevey, Phys. Rev. C **22**, 589 (1980).
 - [22] M. Palacz *et al.*, Nucl. Phys. **A624**, 210 (1997).
 - [23] P.J. Nolan, F.A. Beck, and D.B. Fossan, Annu. Rev. Nucl. Part. Sci. **45**, 561 (1994).
 - [24] R.V.F. Janssens and F.S. Stephens, Nucl. Phys. News **6**, 9 (1996).
 - [25] I-Yang Lee, Nucl. Phys. **A520**, 641c (1990).
 - [26] N.S. Pattabiraman, S.N. Chintalapudi, and S.S. Ghugre, Nucl. Instrum. Methods Phys. Res. A **526**, 432 (2004).
 - [27] N.S. Pattabiraman, S.N. Chintalapudi, and S.S. Ghugre, Nucl. Instrum. Methods Phys. Res. A **526**, 439 (2004).
 - [28] D.C. Radford, Nucl. Instrum. Methods Phys. Res. A **361**, 297 (1995).
 - [29] A. Krämer-Flecken, T. Morek, R.M. Lieder, W. Gast, G. Hebbinghaus, H.M. Jäger, and W. Urban, Nucl. Instrum. Methods Phys. Res. A **275**, 333 (1989).
 - [30] S. Zhu *et al.*, Phys. Rev. C **64**, 041302(R) (2001).
 - [31] Rakesh Popli, F.A. Rickey, and P.C. Simms, Phys. Rev. C **22**, 1121 (1980).
 - [32] D.R. LaFosse *et al.*, Phys. Rev. C **62**, 014305 (2000).
 - [33] H. Schnare *et al.*, Phys. Rev. C **54**, 1598 (1996).
 - [34] F.S. Stephens, R.M. Diamond, J.R. Leigh, T. Kammuri, and K. Nakai, Phys. Rev. Lett. **29**, 438 (1972).
 - [35] S. Raman, C.W. Nestor, and P. Tikkanen, At. Data Nucl. Data Tables **78**, 1 (2001).
 - [36] Eva M. Müller and U. Mosel, J. Phys. G **10**, 1523 (1984).
 - [37] M. Saha, A. Goswami, S. Bhattacharya, and S. Sen, Phys. Rev. C **42**, 1386 (1990).
 - [38] K.P. Lieb *et al.*, Phys. Rev. C **63**, 054304 (2001).
 - [39] S. Bhattacharya, S. Sen, and R.K. Guchhait, Phys. Rev. C **32**, 1026 (1985).
 - [40] A.V. Afanasjev, D.B. Fossan, G.J. Lane, and I. Ragnarsson, Phys. Rep. **322**, 1 (1999).
 - [41] R. Wadsworth *et al.*, Phys. Rev. C **53**, 2763 (1996).
 - [42] R. Wadsworth *et al.*, Phys. Rev. C **50**, 483 (1994).
 - [43] J. Gizon *et al.*, Phys. Lett. **B410**, 95 (1997).
 - [44] J. Simpson *et al.*, Phys. Lett. **B327**, 187 (1994).
 - [45] M. Meyer, J. Danière, J. Letessier, and P. Quentin, Nucl. Phys. **A316**, 93 (1979).

TABLE I: Gamma transition energies (E_γ) in keV, initial and final spins, relative γ ray intensities (I_γ), DCO-ratios (R_{DCO}), and multiplicities for the transitions belonging to ^{103}Cd .

Seq	E_γ (keV)	$J_i^\pi \rightarrow J_f^\pi$	I_γ (Rel.)	R_{DCO}^d	Nature of Gate	Multiplicity
I	118.7(3)	$21/2_1^+ \rightarrow 19/2_1^+$	38.3(37)	0.53(10)	Q	$M1$
	170.4(5)	$25/2_1^+ \rightarrow 23/2_2^+$	10.2(10)	0.52(3)	Q	$M1$
	187.7(2)	$7/2_1^+ \rightarrow 5/2_1^+$	100	0.99(11)	D	$M1$
	208.30(17)	$(31/2_5^+) \rightarrow (31/2_2^+)$	w^a			
	259.1(2)	$27/2_1^+ \rightarrow 25/2_1^+$	32.0(31)	0.49(8)	Q	$M1$
	287.8(3)	$35/2_1^- \rightarrow (35/2_1^+)$	2.9(3)	0.53(13)	Q^b	$E1$
	330.6(5)	$(31/2_5^+) \rightarrow 31/2_1^-$	5.4(5)	0.87(15)	Q	$E1$
	358.7(5)	w^a				
	417.3 ^e	$\rightarrow (31/2_5^+)$	w^a			
	443.7(4)	$(35/2_1^+) \rightarrow (31/2_5^+)$	9.9(10)	0.91(14)	Q	$E2$
	466.60(13)	$(33/2_2^+) \rightarrow (31/2_3^+)$	7.7(7)	0.88(13)	D^b	$M1$
	537.4(3)	$(31/2_3^+) \rightarrow (29/2_4^+)$	0.7(1)	0.88(16)	D^b	$M1$
	562.4 ^e	$\rightarrow (35/2_1^+)$	w^a			
	587.1 ^e	$\rightarrow (31/2_5^+)$	w^a			
	623.2(2)	$19/2_1^+ \rightarrow 15/2_1^+$	61.2(58)	0.99(6)	Q	$E2$
	642.30(11)	$(29/2_4^+) \rightarrow (27/2_3^+)$	4.4(5)	0.97(13)	D^b	$M1$
	673.10(14)	$(31/2_5^+) \rightarrow (29/2_4^+)$	3.7(4)	0.89(15)	D^b	$M1$
	689.2(6)	$25/2_1^+ \rightarrow 21/2_2^+$	0.3(1)			
	694.6(7)	$(35/2_3^+) \rightarrow (33/2_2^+)$	8.2(8)	0.83(11)	D^b	$M1$
	704.10(17)	$(33/2_3^+) \rightarrow (31/2_4^+)$	2.3(3)	0.99(14)	D^b	$M1$
	719.7(2)	$11/2_1^+ \rightarrow 7/2_1^+$	91.2(87)	1.69(5)	D	$E2$
	796.3(7)	$\rightarrow (33/2_3^+)$	w^a			
	811.2(5)	$(29/2_2^+) \rightarrow 27/2_1^+$	10.8(11)	0.76(10)	D	$M1$
	815.6 ^e	w^a				
	841.30(13)	$\rightarrow (27/2_3^+)$	w^a			
	868.30(25)	$(31/2_3^+) \rightarrow (29/2_3^+)$	1.8(2)	0.78(15)	D^b	$M1$
	920.8(2)	$15/2_1^+ \rightarrow 11/2_1^+$	78.7(75)	0.94(3)	Q	$E2$
	942.2(4)	$(31/2_4^+) \rightarrow (29/2_3^+)$	0.10(2)	0.97(18)	D^b	$M1$
	947.50(17)	$(31/2_5^+) \rightarrow (27/2_4^+)$	0.7(1)	0.60(15)	Q^b	$E2$
	963.50(11)	$(27/2_3^+) \rightarrow 25/2_1^+$	5.0(5)	1.04(13)	D^b	$M1$
	1001.10(18)	$(31/2_2^+) \rightarrow (29/2_2^+)$	2.7(3)	0.88(13)	D^b	$M1$
	1004.00(17)	$(31/2_5^+) \rightarrow (29/2_3^+)$	1.8(2)	1.00(21)	D	$M1$
	1015.90(11)	$(29/2_3^+) \rightarrow 27/2_1^+$	5.0(5)	0.43(14)	Q	$M1$
	1025.4(4)	$23/2_2^+ \rightarrow 21/2_1^+$	14.2(13)	1.16(8)	D	$M1$
	1072.90(11)	$(31/2_3^+) \rightarrow (29/2_2^+)$	4.1(4)	0.93(16)	D^b	$M1$
	1108.40(25)	$(31/2_2^+) \rightarrow (27/2_3^+)$	1.1(1)			
	1144.40(16)	$23/2_2^+ \rightarrow 19/2_1^+$	2.6(3)			
	1146.90(22)	$(31/2_4^+) \rightarrow (29/2_2^+)$	1.9(2)	0.85(16)	D^b	$M1$
	1194.5(3)	$25/2_1^+ \rightarrow 21/2_1^+$	27.9(26)	0.99(6)	Q	$E2$
	1210.1 ^e	$\rightarrow (31/2_4^+)$	w^a			
	1332.40(10)	$(27/2_4^+) \rightarrow 25/2_1^+$	1.3(1)	0.86(17)	D^b	$M1$
	1346.70(17)	$(29/2_4^+) \rightarrow 27/2_1^+$	1.0(1)	1.04(17)	D^b	$M1$
	1436.5(3)	$\rightarrow (29/2_2^+)$	0.10(2)			
	1465.3 ^e	$(31/2_5^+) \rightarrow$	w^a			
	1539.5(4)	$(33/2_2^+) \rightarrow (29/2_2^+)$	0.6(1)	0.61(18)	Q^b	$E2$
	1608.60(10)	$(31/2_1^+) \rightarrow 27/2_1^+$	1.0(1)	0.50(18)	Q^b	$E2$
	1712.9 ^e	$\rightarrow (29/2_2^+)$	w^a			
II	187.7(6)	$(19/2_3^+) \rightarrow 19/2_2^+$	2.3(2)			
	449.6(3)	$(25/2_2^+) \rightarrow (23/2_3^+)$	1.5(2)			
	630.70(14)	$0.5(1)$				
	641.1(4)	$\rightarrow 19/2_2^+$	5.6(5)			
	782.4(5)	$19/2_2^+ \rightarrow 15/2_1^+$	13.0(12)	1.18(9)	Q	$E2$
	860.1(9)	$(21/2_3^+) \rightarrow (19/2_3^+)$	8.2(8)	0.56(13)	Q	$M1$
	887.4(6)	$(25/2_2^+) \rightarrow (21/2_3^+)$	9.1(9)	0.95(8)	Q	$E2$

continued...

TABLE I: continued...

Seq	E_γ (keV)	$J_i^\pi \rightarrow J_f^\pi$	I_γ (Rel.)	R_{DCO}^d	Nature of Gate	Multipolarity
III	969.10(11)	$(19/2_3^+) \rightarrow 15/2_1^+$	6.4(6)	0.98(7)	Q	$E2$
	1001.7(8)	$(29/2_6^+) \rightarrow (25/2_2^+)$	10.6(10)	0.88(9)	Q	$E2$
	1046.8(9)	$(21/2_3^+) \rightarrow 19/2_2^+$	4.2(4)	0.53(12)	Q	$M1$
	1099.90(15)	$(27/2_2^+) \rightarrow$	1.4(1)			
	168.4(2)	$11/2_1^+ \rightarrow 9/2_1^+$	1.8(2)	0.56(19)	Q	$M1$
	209.1(4)	$(23/2_1^+) \rightarrow 21/2_1^+$	8.0(8)	0.52(14)	Q	$M1$
	249.7(7)	$(31/2_2^+) \rightarrow (29/2_7^+)$	6.0(6)	0.81(13)	D	$M1$
	256.60(16)	$(27/2_2^+) \rightarrow (23/2_3^+)$	1.7(1)	0.77(14)	Q	$E2$
	270.9(8)	$(35/2_1^+) \rightarrow (33/2_1^+)$	4.6(5)	0.91(16)	D	$M1$
	318.20(11)	$15/2_1^+ \rightarrow 13/2_1^+$	9.6(10)	0.47(29)	Q	$M1$
	318.6(6)	$(31/2_2^+) \rightarrow (29/2_5^+)$	4.4(5)	0.72(18)	D	$M1$
	354.70(15)	$17/2_1^+ \rightarrow 15/2_1^+$	5.1(5)	0.54(23)	Q	$M1$
	380.4(5)	$(33/2_1^+) \rightarrow (31/2_2^+)$	14.0(13)	1.10(26)	D	$M1$
	385.30(14)	$(29/2_7^+) \rightarrow (27/2_5^+)$	3.2(4)	0.80(13)	D^c	$M1$
	415.4(5)	$(35/2_2^+) \rightarrow (33/2_1^+)$	7.7(7)	1.05(28)	D	$M1$
	425.7(6)	$(29/2_1^+) \rightarrow (27/2_2^+)$	10.8(10)	0.49(11)	Q	$M1$
	451.9(9)	$(31/2) \rightarrow (29/2_1^+)$	4.4(5)	0.91(18)	D	D
	551.9(6)	$9/2_1^+ \rightarrow 7/2_1^+$	8.9(9)	0.99(5)	D	$M1$
	604.6(6)	$13/2_1^+ \rightarrow 11/2_1^+$	13.7(13)	0.50(7)	Q	$M1$
	672.3(8)	$17/2_1^+ \rightarrow 13/2_1^+$	10.3(10)	1.01(6)	Q	$E2$
	739.8(8)	$(29/2_5^+) \rightarrow (29/2_1^+)$	6.1(6)	1.92(27)	D	$M1$
	773.1(4)	$13/2_1^+ \rightarrow 9/2_1^+$	32.6(31)	0.84(4)	Q	$E2$
	808.80(18)	$(29/2_7^+) \rightarrow (29/2_1^+)$	2.0(2)	1.89(22)	D	$M1$
	849.30(22)	$(27/2_5^+) \rightarrow (27/2_2^+)$	3.2(4)	1.82(29)	D	$M1$
	892.2(8)	$21/2_2^+ \rightarrow 17/2_1^+$	10.8(10)	0.98(4)	Q	$E2$
	947.8(8)	$19/2_1^- \rightarrow 17/2_1^+$	4.2(4)	0.49(13)	Q	$E1$
	963.4(8)	$(23/2_3^+) \rightarrow 19/2_1^-$	5.3(5)	1.01(15)	Q	$(M2)$
	1182.60(24)	$(29/2_1^+) \rightarrow 23/2_2^+$	1.1(1)			
	1572.90(12)	$(27/2_2^+) \rightarrow (23/2_1^+)$	2.1(2)	0.43(14)	Q^b	$E2$
	1606.3 ^e	$(27/2_5^+) \rightarrow 23/2_2^+$	w^a			
IV	566.10(23)	$\rightarrow 35/2_1^-$	2.3(3)			
	580.3(4)	$\rightarrow 35/2_1^-$	0.60(5)			
	598.2(3)	$\rightarrow 39/2_1^-$	0.80(7)			
	609.9(5)	$\rightarrow 39/2_1^-$	0.70(8)			
	643.1(3)	$15/2_1^- \rightarrow 11/2_1^-$	22.5(21)	0.94(4)	Q	$E2$
	739.9(1)	$9/2_1^+ \rightarrow 5/2_1^+$	64.7(62)	0.88(9)	Q	$E2$
	763.7(4)	$\rightarrow 39/2_1^-$	0.60(7)			
	801.1(4)	$15/2_1^- \rightarrow 13/2_1^+$	19.6(19)	0.51(21)	Q	$E1$
	813.3(3)	$27/2_1^- \rightarrow 23/2_1^-$	37.2(36)	0.97(6)	Q	$E2$
	818.5(1)	$19/2_1^- \rightarrow 15/2_1^-$	41.9(40)	1.82(13)	D	$E2$
	849.4(6)	$\rightarrow 39/2_1^-$	0.30(4)			
	867.4(3)	$23/2_1^- \rightarrow 19/2_1^-$	36.0(34)	0.93(5)	Q	$E2$
	901.4(3)	$31/2_1^- \rightarrow 27/2_1^-$	26.0(25)	0.88(14)	Q	$E2$
	917.2(7)		1.2(2)			
	923.3(2)	$23/2_1^- \rightarrow 21/2_2^+$	0.8(1)			
	930.6(3)	$11/2_1^- \rightarrow 9/2_1^+$	25.9(25)	0.50(14)	Q	$E1$
	1012.4(4)	$\rightarrow 35/2_1^-$	0.30(4)			
	1057.4(6)	$\rightarrow 31/2_1^-$	0.20(3)			
	1063.4(4)	$35/2_1^- \rightarrow 31/2_1^-$	12.9(12)	0.81(18)	Q	$E2$
	1131.5(5)		0.30(4)			
	1151.4(7)	$\rightarrow 39/2_1^-$	0.50(4)			
	1234.2(7)	$39/2_1^- \rightarrow 35/2_1^-$	4.1(4)	0.71(17)	Q	$E2$
	1429.90(14)	$23/2_1^- \rightarrow 21/2_1^+$	1.5(2)			
	1675.1(3)	$\rightarrow 39/2_1^-$	0.40(4)			
	1695.4(6)	$(43/2_1^-) \rightarrow 39/2_1^-$	0.40(4)			$(E2)$
	1713.7(5)	$\rightarrow 39/2_1^-$	0.30(4)			
	1778.4(3)	$\rightarrow 35/2_1^-$	0.40(5)			

continued...

TABLE I: continued...

Seq	E_γ (keV)	$J_i^\pi \rightarrow J_f^\pi$	I_γ (Rel.)	R_{DCO}^d	Nature of Gate	Multipolarity
	2170.6 ^e	$(47/2_1^-) \rightarrow (43/2_1^-)$	w^a			(E2)

[1] a: Corresponds to weak transition whose intensity could not be computed.

[2] b: The transition of interest is used as the gating transition and the cited DCO-value corresponds to the known 119-keV transition. Multipolarity of the gating transition is determined in this process.

[3] c: The transition of interest is used as the gating transition and the cited DCO-value corresponds to the known 250-keV transition. Multipolarity of the gating transition is determined in this process.

[4] d: A blank is left for those transitions for which the R_{DCO} could not be computed.

[5] e: The peak could not be fitted due to poor statistics. The peak energy was determined from the centroid position of the peak and hence the corresponding fitting error could not be computed.

TABLE II: Parameters used for the CPCM calculation for the positive parity levels

Even - even core	Deformation $\delta(= 0.95 \beta_2)$	μ	κ	λ	Δ	Attenuation Factor for the Coriolis Matrix Elements
^{102}Cd	0.14 ^a	0.22 ^b	0.06 ^b	49.0 MeV	1.2 MeV	0.81

^aTaken from the Ref.[22]^bTaken from the Ref.[45]

TABLE III: Comparison of the experimental and theoretical branchings for some of the positive-parity levels. The excitation energies have been expressed in keV. The branchings have been expressed in %. The extreme left column denotes the sequence to which the initial decay state belongs.

Seq	J_i	J_f	E_{x_i}		E_{x_f}		Branching	
			Expt.	(Theo.)	Expt.	(Theo.)	Expt.	[Theo.]
I	11/2 ₁	7/2 ₁	908	(1088)	188	(127)	98.1±13.1	[99.9]
	11/2 ₁	9/2 ₁	908	(1088)	740	(924)	1.9±0.3	[0.1]
I	15/2 ₁	11/2 ₁	1829	(2089)	908	(1088)	89.1±11.4	[99.9]
	15/2 ₁	13/2 ₁	1829	(2089)	1513	(1724)	10.9±1.5	[0.1]
I	23/2 ₂	21/2 ₁	3596	(3779)	2571	(3165)	84.5±10.2	[97.4]
	23/2 ₂	19/2 ₁	3596	(3779)	2452	(2645)	15.5±2.2	[2.6]
I	25/2 ₁	21/2 ₁	3766	(3849)	2571	(3165)	72.7±8.6	[99.2]
	25/2 ₁	23/2 ₂	3766	(3849)	3596	(3779)	26.6±3.2	[0.02]
	25/2 ₁	21/2 ₂	3766	(3849)	3077	(3324)	0.8±0.3	[0.8]
I	29/2 ₄	27/2 ₁	5372	(5733)	4025	(4505)	18.5±2.5	[41.7]
	29/2 ₄	27/2 ₃	5372	(5733)	4730	(5033)	81.5±12.0	[58.3]
I	31/2 ₂	27/2 ₃	5837	(5684)	4730	(5033)	7.7±0.8	[0.2]
	31/2 ₂	29/2 ₂	5837	(5684)	4836	(5287)	19.0±2.4	[99.4]
	31/2 ₂	29/2 ₅	5837	(5684)	5519	(5785)	31.0±4.0	[0.3]
	31/2 ₂	29/2 ₇	5837	(5684)	5588	(6032)	42.3±4.9	[0.1]
I	31/2 ₃	29/2 ₂	5909	(6094)	4836	(5287)	62.1±7.4	[95.2]
	31/2 ₃	29/2 ₄	5909	(6094)	5372	(5733)	10.6±1.7	[0.12]
	31/2 ₃	29/2 ₃	5909	(6094)	5041	(5411)	27.3±3.6	[4.7]
I	31/2 ₄	29/2 ₂	5983	(6370)	4836	(5287)	95.0±13.8	[74.4]
	31/2 ₄	29/2 ₃	5983	(6370)	5041	(5411)	5.0±1.1	[25.6]
I	33/2 ₂	29/2 ₂	6376	(6264)	4836	(5287)	7.2±1.4	[99.9]
	33/2 ₂	31/2 ₃	6376	(6264)	5909	(6094)	92.8±11.6	[0.1]
I	35/2 ₁	31/2 ₅	6489	(6398)	6045	(6446)	68.3±8.7	[26.9]
	35/2 ₁	33/2 ₁	6489	(6398)	6218	(5548)	31.7±4.2	[73.1]
II	19/2 ₃	15/2 ₁	2799	(3088)	1829	(2089)	73.6±8.7	[97.1]
	19/2 ₃	19/2 ₂	2799	(3088)	2611	(2986)	26.4±3.0	[2.9]
II	21/2 ₃	19/2 ₂	3658	(3393)	2611	(2986)	33.9±4.0	[99.6]
	21/2 ₃	19/2 ₃	3658	(3393)	2799	(3088)	66.1±8.0	[0.4]
II	25/2 ₂	21/2 ₃	4545	(4335)	3658	(3393)	85.8±11.3	[68.7]
	25/2 ₂	23/2 ₃	4545	(4335)	4096	(4092)	14.2±2.3	[31.3]
III	9/2 ₁	5/2 ₁	740	(924)	0	(0)	87.9±11.3	[92.4]
	9/2 ₁	7/2 ₁	740	(924)	188	(127)	12.1±1.6	[7.6]
III	13/2 ₁	9/2 ₁	1513	(1724)	740	(924)	70.4±8.4	[66.4]
	13/2 ₁	11/2 ₁	1513	(1724)	908	(1088)	29.6±3.5	[33.6]
III	17/2 ₁	13/2 ₁	2185	(2201)	1513	(1724)	66.9±8.1	[96.9]
	17/2 ₁	15/2 ₁	2185	(2201)	1829	(2089)	33.1±4.0	[3.1]
III	29/2 ₇	29/2 ₁	5588	(6032)	4779	(4666)	38.5±5.1	[90.0]
	29/2 ₇	27/2 ₅	5588	(6032)	5202	(5368)	61.5±9.4	[10.0]

FIG. 1: “(Color online)” Part of the proposed level scheme, including *Seq* I, for ^{103}Cd as obtained from the present work.

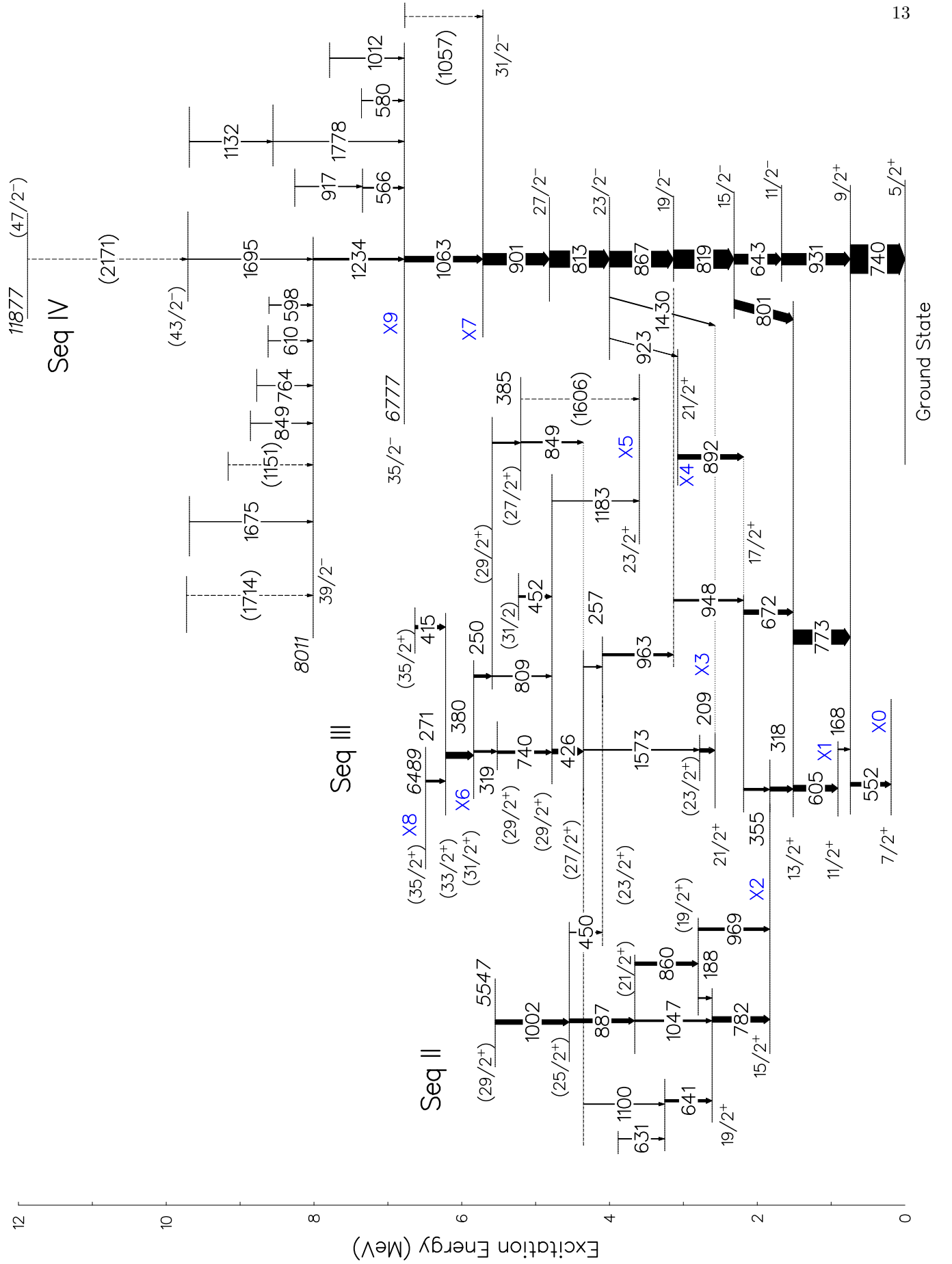


FIG. 2: “(Color online)” Part of the proposed level scheme, including Seq II, III, and IV, for ^{103}Cd as obtained from the present

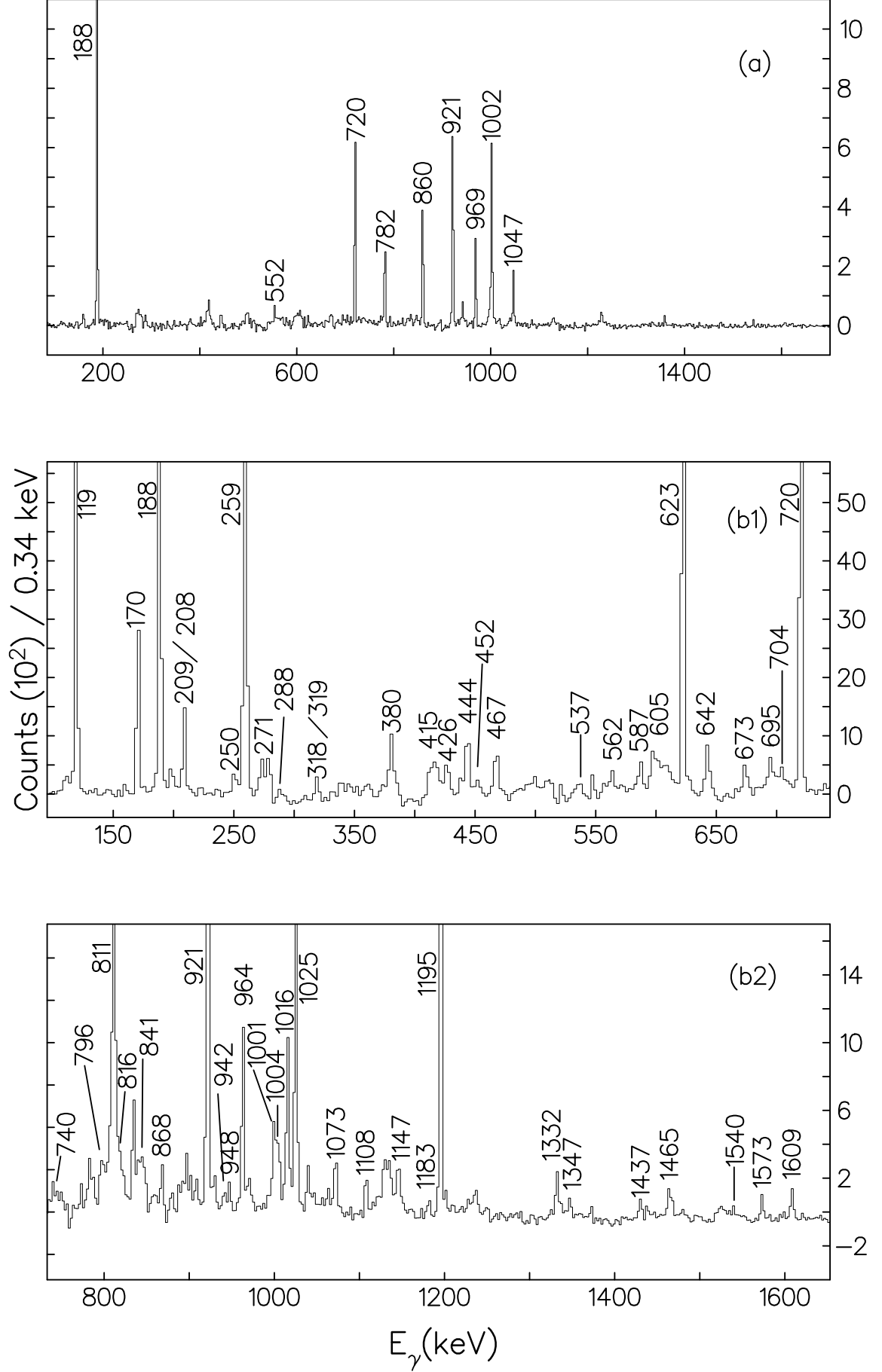


FIG. 3: (a) Representative $\gamma\gamma\gamma$ coincidence spectra of the 887-keV transition with other members of *Sea II*. (b1-b2) Coin-

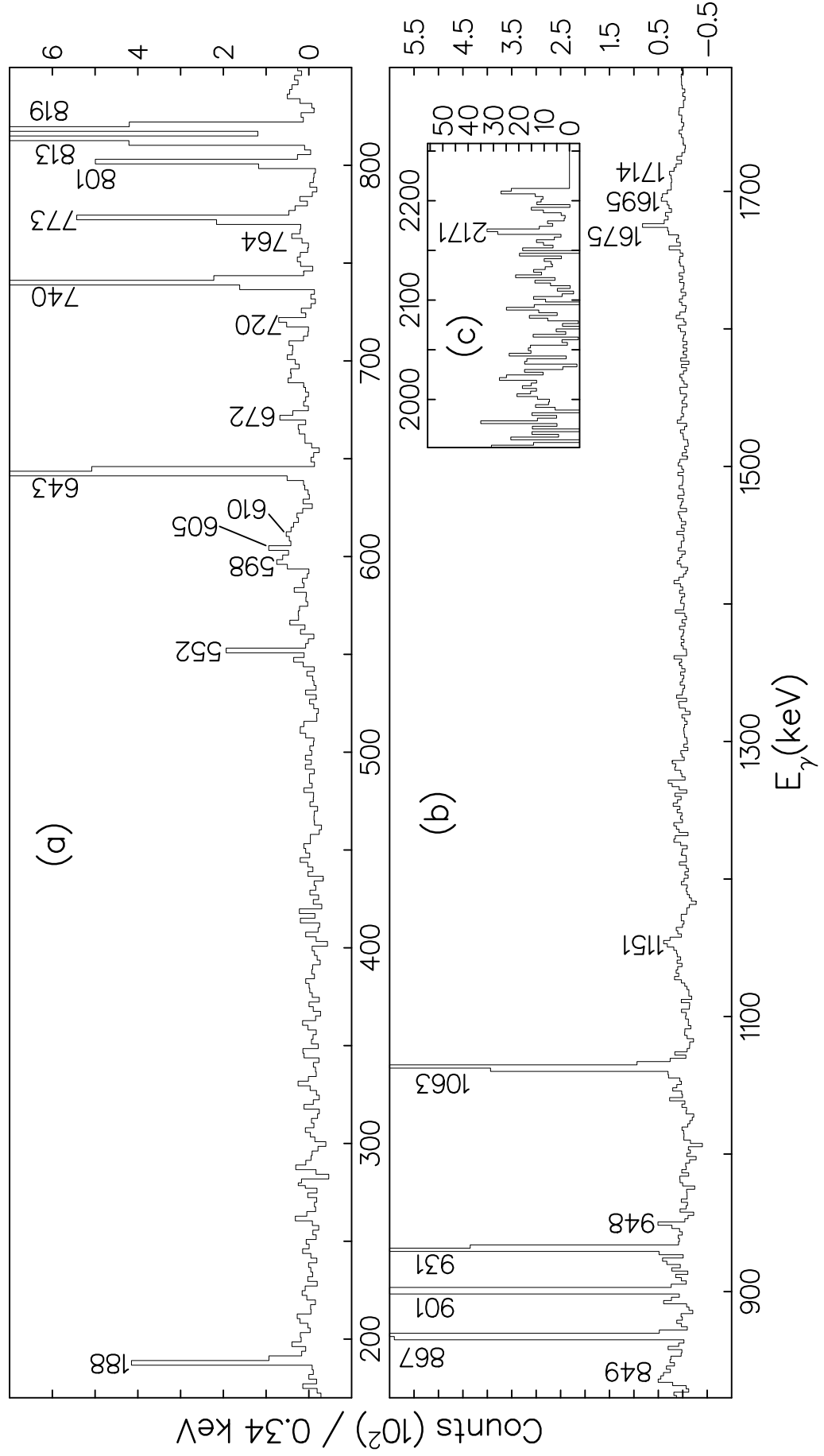


FIG. 4: (a-b) Representative $\gamma\gamma\gamma$ coincidence spectra of the 1234-keV transition with other members of *Seq IV*. Peaks labeled

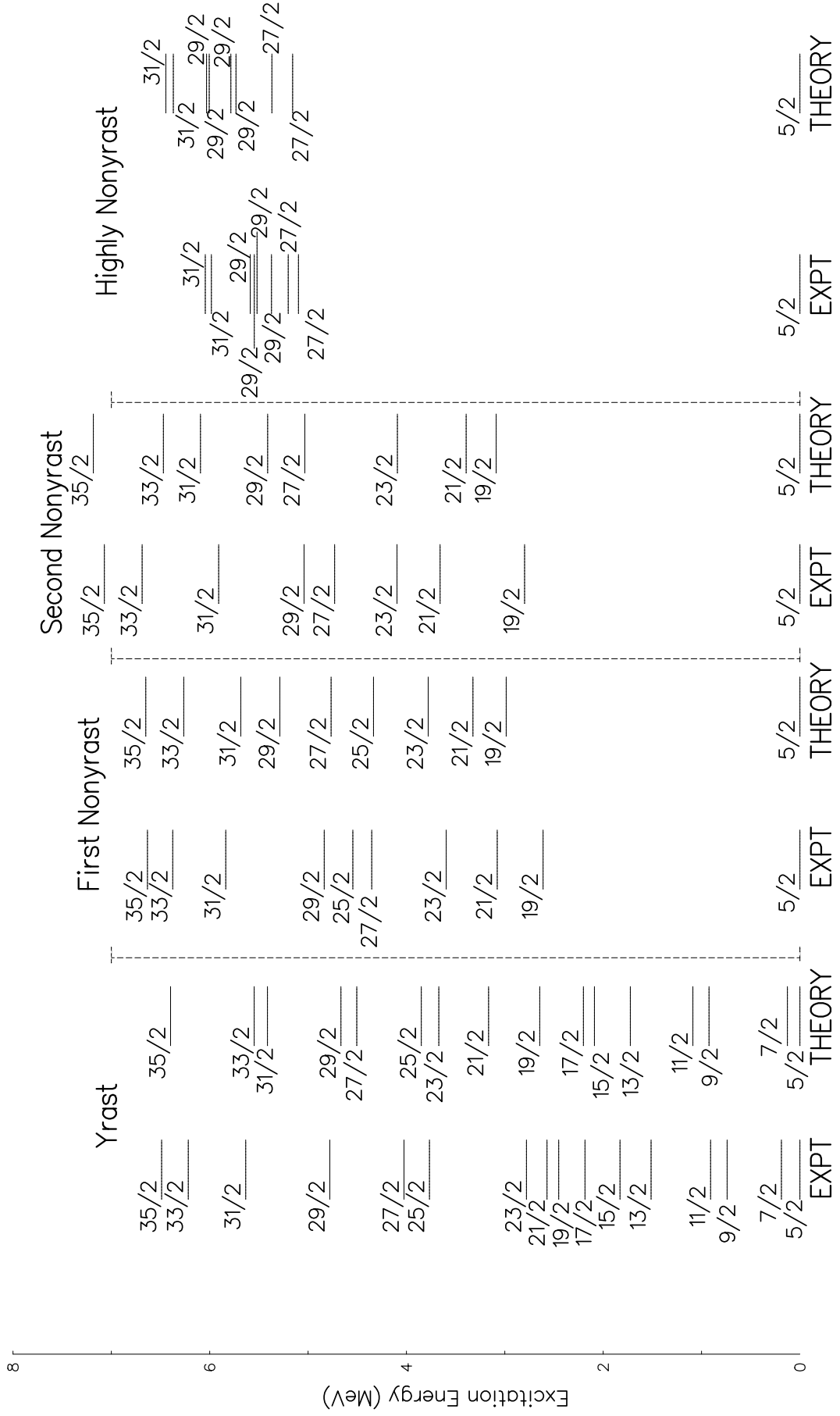


FIG. 5: Comparison of the positive-parity levels of ^{103}Cd with the predictions of CPCM calculations; see text for details.

	47/2 ⁻ 10206	
		47/2 ⁻ 9756
47/2 ⁻ 8442		43/2 ⁻ 8473
	43/2 ⁻ 8035	
43/2 ⁻ 7224		39/2 ⁻ 7266
39/2 ⁻ 6193	39/2 ⁻ 6340	35/2 ⁻ 6139
35/2 ⁻ 4822	35/2 ⁻ 5106	31/2 ⁻ 4914
31/2 ⁻ 3970	31/2 ⁻ 4043	27/2 ⁻ 3895
27/2 ⁻ 3086	27/2 ⁻ 3142	23/2 ⁻ 3006
23/2 ⁻ 2204	23/2 ⁻ 2329	19/2 ⁻ 2079
19/2 ⁻ 1495	19/2 ⁻ 1462	15/2 ⁻ 1195
15/2 ⁻ 686	15/2 ⁻ 643	
11/2 ⁻ 0	11/2 ⁻ 0	11/2 ⁻ 0
THEORY (PROLATE)	EXPT	THEORY (OBLATE)

FIG. 6: Comparison of the experimental and theoretical excitation energies of negative-parity levels in ^{103}Cd . Energies of the levels are labeled in keV. The calculations have been carried out with both the prolate and oblate deformation of the core (see text for details). The states with the prolate deformation are found to be dominated by the Nilsson basis states $1/2[550]$ (= 82% $\nu h_{11/2}$), $3/2[541]$ (= 88% $\nu h_{11/2}$), and $5/2[532]$ (= 93% $\nu h_{11/2}$) contributing about 50 - 60%, 30%, and 10%, respectively. The states with the oblate deformation are found to be dominated by the Nilsson basis states $11/2[505]$ (= 100% $\nu h_{11/2}$), $9/2[514]$ (= 99% $\nu h_{11/2}$), and $7/2[523]$ (= 86% $\nu h_{11/2}$) contributing about 60 - 85%, 10 - 25%, and 2 - 10%, respectively.

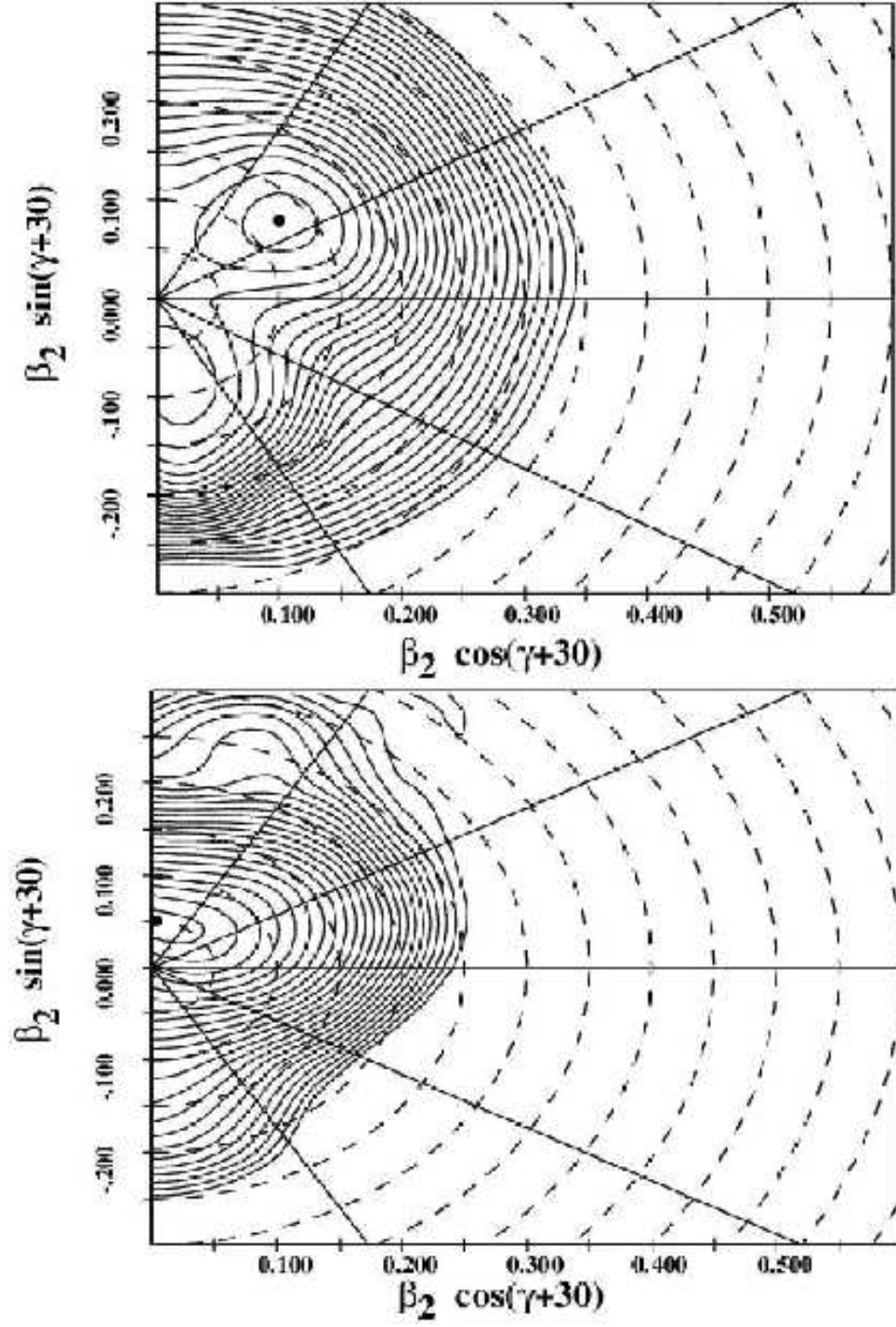


FIG. 7: TRS calculations for states of parity and signature, $(\pi, \alpha) = (-, -1/2)$, showing the development of energy minima. Top panel: $\hbar\omega = 0.35$ MeV; minimum at $\beta_2 = 0.13$, $\gamma = 8^\circ$. Bottom panel: $\hbar\omega = 0.70$ MeV; minimum at $\beta_2 = 0.05$, $\gamma = 57^\circ$.

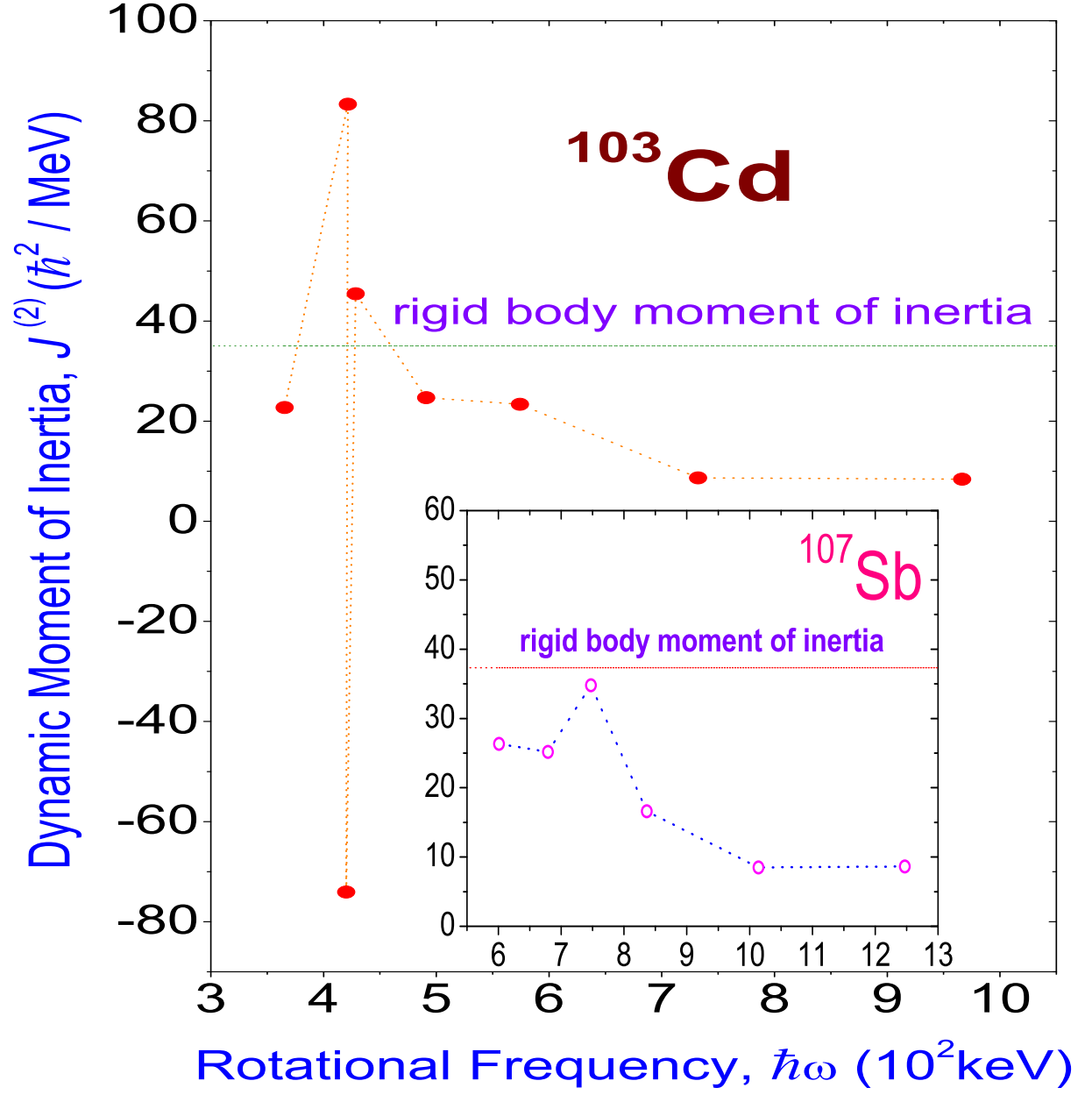


FIG. 8: “(Color online)” The dynamic moment of inertia for *Seq. IV* in ^{103}Cd . The dashed line corresponds to the moment of inertia for a rigid body having mass $A = 103$ and deformation $\beta_2 = 0.23$. The inset shows the same for ^{107}Sb [32].